VIII ECCOMAS Thematic Conference on Smart Structures and Materials
SMART 2017
A. Güemes, A. Benjeddou, J. Rodellar and J. Leng (Eds)

NON-LINEAR ANALYSIS OF A PRE-STRESSED PIEZOELECTRIC MULTI-LAYER PLATE

FLORIAN TOTH[*], MANUEL DORFMEISTER[†], MICHAEL SCHNEIDER[†], ULRICH SCHMID[†] AND MANFRED KALTENBACHER[*]

[*]Institute of Mechanics and Mechatronics
TU Wien
Getreidemarkt 9, 1060 Vienna, Austria
e-mail: florian.toth@tuwien.ac.at, web page: http://www.mec.tuwien.ac.at/

[†] Institute of Sensor and Actuator Systems
TU Wien
Gusshausstrasse 27-27, 1040 Vienna, Austria
web page: http://www.isas.tuwien.ac.at/

Key words: MEMS, Piezo, Pre-Stress, Circular Plate

Abstract. A geometrically non-linear mechanical model for a MEMS actuator is developed based on von Karman plate theory. Piezoelectric and thermally stressed layers are incorporated within the framework of classical lamination theory. The formulation is completely general with respect to the possible configuration of layers. It is then employed to treat circular plates under the assumption of axially-symmetric deformations. Finally, some results for a selected piezo-actuator are presented.

1 INTRODUCTION

Loss of stability through buckling or snap-through is usually undesired in engineering structures. However, buckling phenomena can also be exploited e.g. to determine material parameters through indirect experiments [1], or in actuator applications [2]. While the determination of critical loads (i.e. the load at which a bifurcation occurs) is often sufficient for the prevention against the loss of stability in standard applications, the exploitation of buckling phenomena in actuator applications requires precise knowledge about the post-critical behaviour of the investigated system.

This makes geometrically non-linear formulation necessary. The simplest of such formulations is based on von Karman plate theory, resulting in a set of equations which is difficult to solve [3, 4, 5]. For the case of circular, isotropic plates it is possible to prove the existence of a solution to the von Karman plate equations [6]. Considerable simplification is possible by employing Berger's approximation [5, 7]. Originally developed for isotropic plates, it can also be applied to composite plates without coupling stiffness matrix [8]. The challenging nature of the von Karman equations has inspired the development of many numerical methods [9, 10, 11, 12, 13]. The incorporation of piezoelectric layers into classical lamination theory can be done in a straightforward manner [14, 15].

The investigated microelectromechanical system (MEMS) consists of a circular, multilayer plate with the intended use as an actuator for digital sound reconstruction (DSR). The multilayer structure is pre-stressed due to the production process leading to buckling of the plate structure. The piezo layer is actuated to switch from one to the other stable equilibrium. The advantage of such an actuator exploiting the post-buckling behaviour is a significantly larger stroke level.

2 MECHANICAL MODEL

One of the key points of the mechanical modelling of the actuator system is the correct description of the electromechanical coupling including pre-stress. In order to accurately describe the post-buckling behaviour we require a large-displacement framework. However, the model must be simple enough to enable a mathematical analysis of the non-linear behaviour of the structure to be suitable for the tailored design of actuators. In order to obtain a computationally efficient model the multi-layer structure will be treated as a thin plate.

2.1 Plate Kinematic

Adopting the Kirchhoff hypothesis we can describe the strain state in the plate by

$$\bar{\boldsymbol{\epsilon}} = \boldsymbol{\epsilon} + z\boldsymbol{\kappa}, \tag{1}$$

where the in-plane strain tensor $\boldsymbol{\epsilon}$ and the curvature tensor $\boldsymbol{\kappa}$ describe the deformation of the reference surface of the plate, and z is transverse coordinate measured from the reference surface. We choose to use the von Karman assumptions to derive the simplest possible geometrically non-linear plate formulation. Thus, we write the deformation tensors of the reference surface as

$$\begin{aligned} \boldsymbol{\epsilon} &= \frac{1}{2}\left(\boldsymbol{\nabla u} + (\boldsymbol{\nabla u})^T + \boldsymbol{\nabla} u_3 \boldsymbol{\nabla} u_3\right), & (2)\\ \boldsymbol{\kappa} &= -\boldsymbol{\nabla\nabla} u_3, & (3) \end{aligned}$$

with the displacement vector $\boldsymbol{u} = [u_1, u_2, u_3]$. The above formulation allows the coupling of transverse displacements, i.e. u_3, and in-plane strains.

2.2 Constitutive Model

As we are dealing with a thin plate we assume a plane stress state with a vanishing normal stress in thickness direction. All materials are modelled as transversally isotropic with the axis of the vanishing normal stress perpendicular to the isotropic plane. Employing Voigts linearised theory of piezoelectricity and additionally considering thermal strains we can write the linearised constitutive relation as

$$\begin{aligned} \underbrace{\begin{bmatrix} \sigma_{11} \\ \sigma_{22} \\ \sigma_{12} \end{bmatrix}}_{\bar{\boldsymbol{\sigma}}} &= \underbrace{\begin{bmatrix} Q_{11} & Q_{12} & 0 \\ Q_{12} & Q_{11} & 0 \\ 0 & 0 & Q_{66} \end{bmatrix}}_{\bar{\boldsymbol{C}}} \underbrace{\begin{bmatrix} \epsilon_{11} \\ \epsilon_{22} \\ 2\epsilon_{12} \end{bmatrix}}_{\bar{\boldsymbol{\epsilon}}} - \bar{\boldsymbol{C}} \underbrace{\begin{bmatrix} \alpha_1 \\ \alpha_1 \\ 0 \end{bmatrix}}_{\bar{\boldsymbol{\alpha}}} \Delta T - \underbrace{\begin{bmatrix} \bar{e} \\ \bar{e} \\ 0 \end{bmatrix}}_{\bar{\boldsymbol{e}}^T} E_3, & (4)\\ D_3 &= \bar{\boldsymbol{e}}\bar{\boldsymbol{\epsilon}} - \bar{\boldsymbol{e}}\bar{\boldsymbol{\alpha}}\Delta T + \bar{\eta} E_3, & (5) \end{aligned}$$

where $\bar{\boldsymbol{\sigma}}$ is the plane stress tensor (in Voigt notation), ΔT is the temperature change with respect to a reference temperature, E_3 is the electric field strength in thickness direction and D_3 is the dielectric displacement in thickness direction. The components Q_{ij} of the effective plane-stress stiffness tensor $\bar{\boldsymbol{C}}$ can be computed from the components C_{ij} of the transversally isotropic stiffness tensor by

$$Q_{11} = C_{11} - \frac{C_{13}^2}{C_{33}}, \qquad Q_{12} = C_{12} - \frac{C_{13}^2}{C_{33}}, \qquad Q_{66} = \frac{C_{11} - C_{12}}{2}, \tag{6}$$

and the components of the effective plane-stress piezoelectric coupling tensor $\bar{\boldsymbol{e}}$ as well as the effective plane-stress permittivity $\bar{\eta}$ are given by

$$\bar{e} = e_{31} - \frac{C_{13}}{C_{33}} e_{33}, \qquad \bar{\eta} = \eta_{33} + \frac{e_{33}^2}{C_{33}}, \tag{7}$$

where e_{ij} and η_{ij} denote the entries of the transversally isotropic piezoelectric coupling and electric permittivity tensors, respectively.

We have already neglected any electric field components in in-plane direction. Therefore, Gauss' law simplifies to $\partial D_3/\partial z = 0$, stating that the dielectric displacement is constant in each layer. We can now insert the kinematic assumption (1) into (5) and integrate over the layer thickness Δz to obtain

$$D_3 = \frac{1}{\Delta z} \int D_3 \,\mathrm{d}z = \bar{\boldsymbol{e}}\boldsymbol{\epsilon} + \bar{z}\bar{\boldsymbol{e}}\boldsymbol{\kappa} - \bar{\boldsymbol{e}}\bar{\boldsymbol{\alpha}}\Delta T + \bar{\eta}\frac{\Delta V}{\Delta z}, \tag{8}$$

where $\bar{z}$ denotes the vertical coordinate of the middle of the layer and ΔV the voltage difference applied to the electrodes at the top and bottom of the layer [8, 15]. Reinserting back into (5) yields

$$E_3 = \frac{\bar{z} - z}{\bar{\eta}} \bar{\boldsymbol{e}}\boldsymbol{\kappa} + \frac{\Delta V}{\Delta z}, \tag{9}$$

which is finally inserted into (4). Thus, the constitutive relation for each layer reads

$$\bar{\boldsymbol{\sigma}} = \bar{\boldsymbol{C}}\boldsymbol{\epsilon} + z\left(\bar{\boldsymbol{C}} - (\bar{z} - z)\bar{\boldsymbol{E}}\right)\boldsymbol{\kappa} - \boldsymbol{\tau}, \tag{10}$$

where the tensor

$$\bar{\boldsymbol{E}} = \frac{\bar{\boldsymbol{e}}^T \bar{\boldsymbol{e}}}{\bar{\eta}}, \tag{11}$$

accounts for stiffening due to the equipotential conditions on the electrodes of the piezo. For non-piezoelectric layers the coupling tensor is zero and thus there is no stiffening. The stress components due to piezo actuation or temperature change are included via

$$\boldsymbol{\tau} = \bar{\boldsymbol{C}}\bar{\boldsymbol{\alpha}}\Delta T + \bar{\boldsymbol{e}}^T \frac{\Delta V}{\Delta z}. \tag{12}$$

It is interesting to note that both effects can be treated with the same forcing term in the constitutive equation.

As a last step we integrate (10) over the thickness of the plate to obtain the constitutive relation on the plate level

$$\begin{bmatrix} \boldsymbol{n} \\ \boldsymbol{m} \end{bmatrix} = \begin{bmatrix} \boldsymbol{A} & \boldsymbol{B} \\ \boldsymbol{B} & \boldsymbol{D} \end{bmatrix} \begin{bmatrix} \boldsymbol{\epsilon} \\ \boldsymbol{\kappa} \end{bmatrix} - \begin{bmatrix} \tilde{\boldsymbol{n}} \\ \tilde{\boldsymbol{m}} \end{bmatrix}, \tag{13}$$

which relates the section forces and moments $\boldsymbol{n}$ and $\boldsymbol{m}$ defined as

$$\boldsymbol{n} = \sum_l \int \bar{\boldsymbol{\sigma}}_l \,\mathrm{d}z, \qquad \boldsymbol{m} = \sum_l \int z \bar{\boldsymbol{\sigma}}_l \,\mathrm{d}z, \tag{14}$$

to the deformation of the reference surface via the in-plane stiffens matrix $\boldsymbol{A}$, the coupling stiffness matrix $\boldsymbol{B}$, and the bending stiffness matrix $\boldsymbol{D}$, well known from classical lamination theory. The section forces and moments due to the combined effect of piezo actuation and thermal stress are included via $\tilde{\boldsymbol{n}}$ and $\tilde{\boldsymbol{m}}$, respectively. They are computed equivalently to (14) by replacing $\bar{\boldsymbol{\sigma}}$ with $\boldsymbol{\tau}$. The laminate stiffness matrices are

$$\boldsymbol{A} = \sum_l \int \bar{\boldsymbol{C}} \,\mathrm{d}z = \sum_l \Delta z_l \bar{\boldsymbol{C}}_l, \tag{15}$$

$$\boldsymbol{B} = \sum_l \int z \left(\bar{\boldsymbol{C}} - (\bar{z} - z)\bar{\boldsymbol{E}}\right) \mathrm{d}z = \sum_l \bar{z}_l \Delta z_l \bar{\boldsymbol{C}}_l, \tag{16}$$

$$\boldsymbol{D} = \sum_l \int \left(z^2(\bar{\boldsymbol{C}}_l + \bar{\boldsymbol{E}}_l) - z\bar{z}_l\bar{\boldsymbol{E}}_l\right) \mathrm{d}z = \sum_l \frac{\Delta z_l^3}{12}\left(\bar{\boldsymbol{C}}_l + \bar{\boldsymbol{E}}_l\right) - \bar{z}^2 \Delta z \left(\bar{\boldsymbol{C}}_l + 2\bar{\boldsymbol{E}}_l\right), \tag{17}$$

with the abbreviations

$$\Delta z_l = z_{l+1} - z_l, \qquad \bar{z}_l = \frac{z_{l+1} + z_l}{2}, \tag{18}$$

for the layer thickness and center coordinate.

2.3 Equilibrium Equations

We neglect any in-plane forces other than the ones introduced by piezo actuation or temperature change. Furthermore, we only consider the static equilibrium. The equilibrium equations can then be written as

$$\boldsymbol{\nabla} \cdot \boldsymbol{n} = 0, \tag{19}$$

$$\boldsymbol{\nabla} \cdot \boldsymbol{\nabla} \cdot \boldsymbol{m} + \boldsymbol{\nabla} \cdot (\boldsymbol{n} \cdot \boldsymbol{\nabla} u_3) - p_3 = 0, \tag{20}$$

where p_3 denotes a pressure acting transverse to the plate [8].

We now introduce a cylindrical coordinate system with its origin in the center of the plate. Restricting ourselves to rotationally symmetric loading, and thus deformations and section forces and moments, above partial differential equations are reduced to a set of coupled ordinary differential equations with respect to the radial coordinate r. Applying the divergence and gradient operators in cylindrical coordinates in (19) and (20) one obtains

$$n_r' + \frac{n_r - n_\phi}{r} = 0, \tag{21}$$

$$\left(r m_r' + m_r - m_\phi\right)' + \left(r m_r u_z'\right)' + p_z r = 0, \tag{22}$$

for the non-trivial components, where the indices r, ϕ and z indicate the radial and circumferential and axial direction and $()'$ denotes the derivative with respect to r. The above moment equation can be easily integrated once [16, 17] to obtain

$$2\left(rm_r' + m_r - m_\phi + rm_r u_z'\right) + p_z r^2 \quad = \quad 0. \tag{23}$$

Inserting the deformation measures (2) and (3) for axially symmetric deformations of the reference surface in cylindrical coordinates into (13) on obtains the following expressions for section forces and moments

$$n_r = \frac{A_{r\phi}u_r}{r} + A_{rr}u_r' - \frac{B_{r\phi}u_z'}{r} + \frac{A_{rr}u_z'^2}{2} - B_{rr}u_z'' - \bar{n}, \tag{24}$$

$$n_\phi = \frac{A_{rr}u_r}{r} + A_{r\phi}u_r' - \frac{B_{rr}u_z'}{r} + \frac{A_{r\phi}u_z'^2}{2} - B_{r\phi}u_z'' - \bar{n}, \tag{25}$$

$$m_r = \frac{B_{r\phi}u_r}{r} + B_{rr}u_r' - \frac{D_{r\phi}u_z'}{r} + \frac{B_{rr}u_z'^2}{2} - D_{rr}u_z'' - \bar{m}, \tag{26}$$

$$m_\phi = \frac{B_{rr}u_r}{r} + B_{r\phi}u_r' - \frac{D_{rr}u_z'}{r} + \frac{B_{r\phi}u_z'^2}{2} - D_{r\phi}u_z'' - \bar{m}. \tag{27}$$

These can now be inserted into (21) and (23) to obtain two non-linearly coupled ordinary differential equations (ODEs) of third order in $u_z(r)$ and second-order in $u_r(r)$.

As boundary conditions at the center, i.e. $r = 0$ and the outer radius $r = R$ we require

$$u_r(0) = 0, \quad u_z'(0) = 0, \quad u_z(R) = 0, \quad n_r(R) = -k_n u_r(R), \quad m_r(R) = k_m u_z'(R), \tag{28}$$

where we have introduced the boundary stiffness factors k_n and k_m. These can be used to transit between simply supported and freely movable in radial direction, i.e. $k_m \to 0$ and $k_n \to 0$, to clamped, i.e. $k_m \to \infty$ and $k_n \to \infty$, behaviour. The clamped behaviour can of course also be enforced by requiring

$$u_z'(R) = 0, \quad \text{and} \quad u_r(R) = 0. \tag{29}$$

The latter is mathematically exact, the former can be seen as a penalty formulation.

The coupled second and third order ODEs can be cast into a system of first order ODEs by introducing axillary variables for the derivatives. The resulting system of 5 non-linearly coupled first order ODEs, $\boldsymbol{y}'(r) = \boldsymbol{f}(\boldsymbol{y}, r)$ with $\boldsymbol{y} = [u_z'', u_z', u_z, u_r', u_r]^T$ and boundary conditions $\boldsymbol{g}(\boldsymbol{y}(0), \boldsymbol{y}(R)) = \boldsymbol{0}$, can then be solved numerically. This is for example possible by the shooting method [18]. In the current work we employ a collocation based boundary value problem solver [19]. For the numerical solution one has to consider that the equations have a singularity at $r \to 0$. However, knowing that the physical solution must be bounded, we can form the limits $\lim\limits_{r\to 0} \boldsymbol{f}$ and $\lim\limits_{r\to 0} \boldsymbol{g}$ by the application of L'Hôpital's rule.

3 ACTUATOR CONFIGURATION

As an example we consider an circular actuator with a diameter of 800 µm as shown in Fig. 1. The plate consists of a 2 µm thick Silicon (Si) substrate, including a 200 nm thick a-SiC:H 'stress-layer' which is used to adapt the pre-stress of the system in the production process. The electrodes surrounding the 400 nm Aluminium-Nitride (AlN) piezo layer consist of 50 nm

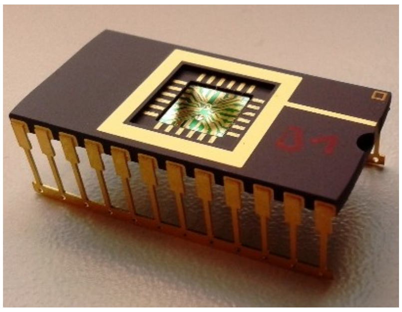

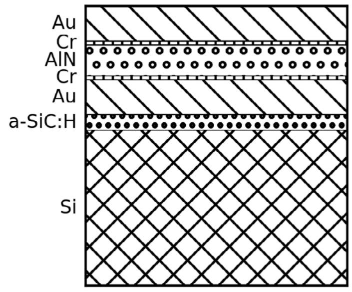

Figure 1: Chip with MEMS actuator (left); Top view of the actuator showing the electrode configuration (center); Material layers assumed in the analysis (right).

Table 1: Assumed values for the material parameters.

	Q_{11}/Pa	Q_{12}/Pa	$\bar{e}$/Cm^{-2}	$\bar{\eta}$/Fm^{-1}	α/K^{-1}
Si	1.93e+11	5.02e+10			
a-SiC:H	1.93e+11	5.02e+10			2.60e-06
Au	9.40e+10	3.76e+10			
Cr	3.07e+11	9.20e+10			
AlN	3.55e+11	1.00e+11	-2.75e+00	1.26e-10	

Chromium (Cr) and 450 nm Gold (Au). Thus, we have a total thickness of $h = 3.6$ µm. The assumed material properties are given in Tab. 1.

To take into account the electrode configuration of the actuator (as can be seen in Fig. 1) one needs to consider the possibility of radially varying actuation voltages. The center electrode might have a different actuation voltage as the outer ring shaped-electrode. In order to avoid numerical difficulties we assume smooth transitions between actuation voltages by combining tanh-functions.

4 RESULTS

In a first step we investigate the impact of different actuation schemes on the resulting deformation of the composite plate. Three different actuations are considered: First only the center electrode is actuated. In the second configuration the center electrode and the ring electrode are actuated in different directions, i.e. with a negative and positive voltage, respectively. In the third configuration we assume that the ring electrode ends before the outer radius of the plate, thus the actuation voltage is zero at this location. The shape of the total actuation voltage and the resulting deformation of the actuator are depicted in Fig. 2. For the case of free rotation at the outer edge (simply supported) the bending moment introduced by the piezo actuation leads to curvature of the plate. The negative voltage at the center electrode leads to a positive curvature and thus to a displacement in negative z-direction. If the positive voltage of the ring electrode is added the resulting negative curvature leads to an overall positive vertical displacement. The behaviour is dominated by the larger ring electrode. If the ring electrode

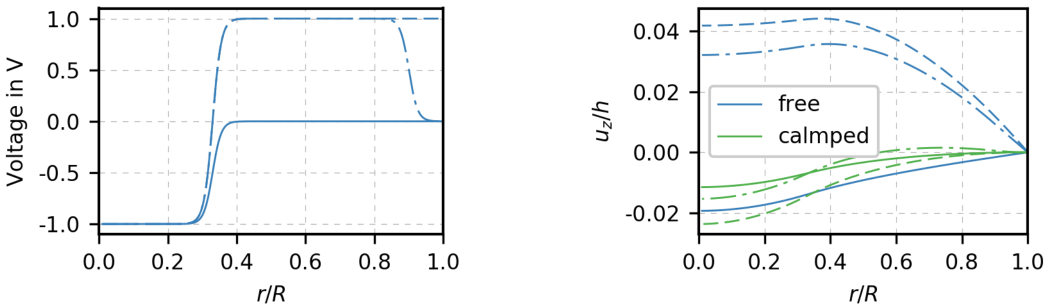

Figure 2: Impact of the electrode configuration on the deformation shape: Level of the actuation voltage (left); and resulting deformation shape for different boundary conditions (right).

ends before the outer edge of the plate the total displacement is slightly smaller. For a clamped outer edge the behaviour is different: The boundary condition does not allow for any deformation due to constant piezo actuation (provided it is below the buckling load). However, the change of actuation gradient of the actuation voltage between center electrode and ring electrode causes a deformation of the actuator. The internal forcing introduced by the actuation is similar to an external moment at the transition between the electrodes. The overall displacement is significantly smaller in the case of a clamped outer edge.

Finally, we explore the effect of compressible residual stress introduced in the stress-layer. In the current case this is modelled as thermal expansion. The temperature is therefore regarded as a loading parameter, which could be different for different effects introducing the residual stress. On the level of the plate the residual stresses in the layers lead to residual section forces and moments. Once the critical section force is reached the plate can buckle. As the configuration is un-symmetric, i.e. we have a non-zero $\boldsymbol{B}$-matrix, there exists a preferred buckling direction. As can be seen from the bifurcation diagram in Fig. 3 this is the upper side for the investigated configuration. The diagram shows the typical pitchfork bifurcation as expected for a plate. Observing the sharpness of the bifurcation one can conclude that the imperfection due to the unsymmetrical stacking of layers is small. Once the critical load is exceeded, several equilibrium positions may exist. Further increasing the load up to the second buckling load one can recognise additional buckling mode shapes. It should be noted that, transitions between the different branches due to snap-buckling [8] cannot be treated within the assumption of an axially-symmetric deformation.

5 CONCLUSIONS

A formulation for piezoelectric plate actuators has been presented. The mathematically equivalent effects of thermal stress and piezo actuation are included into the formulation by a modified constitutive law, which can be incorporated into classical lamination theory in a straight forward manner. The equilibrium equations based on the von Karman plate theory for circular plates with axially-symmetric deformation shape were derived for general un-symmetric laminates. The resulting non-linear, coupled ODEs were then solved numerically to obtain the deformed actuator configuration for different electrode actuations. Comparison of the impact

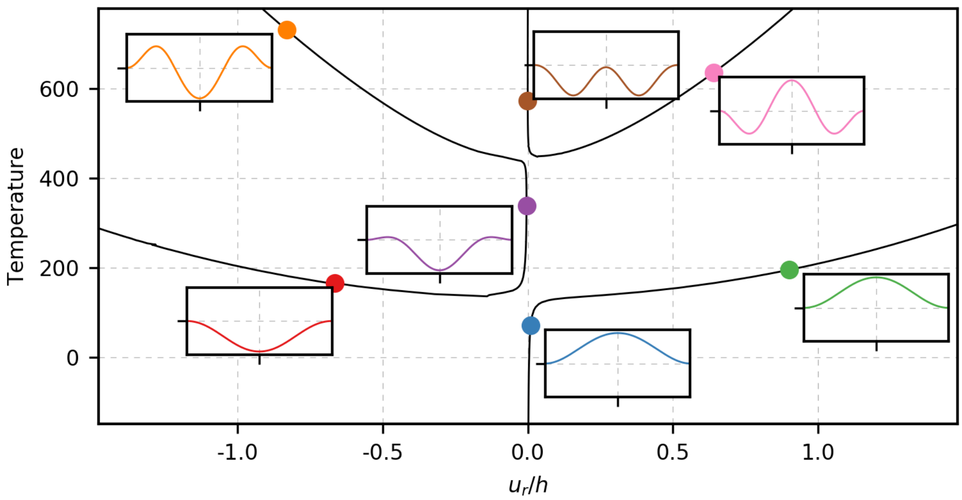

Figure 3: Bifurcation diagram of center displacement versus temperature in the stress-layer as loading parameter. The shape of the actuator for selected equilibrium points is shown as inserts.

of the boundary condition at the outer edge demonstrated the importance of correct modelling assumptions in therms of an equivalent boundary stiffness. Finally, a bifurcation plot for the investigated actuator was created using the temperature in a 'stress-layer' as the loading parameter.

The proposed modelling strategy is computationally inexpensive. It can be naturally applied to arbitrary layered configurations. It offers great flexibility in the incorporation of actuation patters and the treatment of boundary conditions at the edge of the plate. Therefore, it shows potential for the tailored design of actuators.

References

[1] Wilder, E.A., Guo, S., Lin-Gibson, S., Fasolka, M.J., and Stafford, C.M., Measuring the modulus of soft polymer networks via a buckling-based metrology, *Macromolecules* (2006) **39**(12):4138–4143.

[2] Yang, D., Mosadegh, B., Ainla, A., Lee, B., Khashai, F., Suo, Z., Bertoldi, K., and Whitesides, G.M., Buckling of elastomeric beams enables actuation of soft machines, *Advanced Materials* (2015) **27**(41):6323–6327.

[3] Coman, C.D., On the compatibility relation for the Föppl–von Kármán plate equations, *Applied Mathematics Letters* (2012) **25**(12):2407–2410.

[4] Chia, C.Y., Geometrically nonlinear behavior of composite plates: A review, *Applied Mechanics Reviews* (1988) **41**(12):439.

[5] Villaggio, P., *Mathematical Models for Elastic Structures.* Cambridge University Press (CUP) (1997).

[6] Dickey, R.W., Nonlinear bending of circular plates, *SIAM Journal on Applied Mathematics* (1976) **30**(1):1–9.

[7] Berger, H.M., *A new approach to the analysis of large deflections of plates.* PhD thesis, California Institute of Technology, (1954).

[8] Krommer, M., Vetyukov, Y., and Staudigl, E., Nonlinear modelling and analysis of thin piezoelectric plates: Buckling and post-buckling behaviour, *Smart Structures and Systems* (2016) **18**(1):155–181.

[9] Dai, H.H., Paik, J.K., and Atluri, S.N., The global nonlinear galerkin method for the analysis of elastic large deflections of plates under combined loads: A scalar homotopy method for the direct solution of nonlinear algebraic equations, *Computers, Materials & Continua* (2011) **23**(1):69–100.

[10] Kirby, R. and Yosibash, Z., Solution of von-kármán dynamic non-linear plate equations using a pseudo-spectral method, *Computer Methods in Applied Mechanics and Engineering* (2004) **193**(6-8):575–599.

[11] Wang, X., Liu, X., Wang, J., and Zhou, Y., A wavelet method for bending of circular plate with large deflection, *Acta Mechanica Solida Sinica* (2015) **28**(1):83–90.

[12] Azrar, L., Boutyour, E.H., and Potier-Ferry, M., Non-linear forced vibrations of plates by an asymptotic-numerical method, *Journal of Sound and Vibration* (2002) **252**(4):657–674.

[13] Kamiya, N., Sawaki, Y., Nakamura, Y., and Fukui, A., An approximate finite deflection analysis of a heated elastic plate by the boundary element method, *Applied Mathematical Modelling* (1982) **6**(1):23–27.

[14] Krommer, M., The significance of non-local constitutive relations for composite thin plates including piezoelastic layers with prescribed electric charge, *Smart Materials and Structures* (2003) **12**(3):318–330.

[15] Reddy, J.N., *Mechanics of Laminated Composite Plates and Shells: Theory and Analysis, Second Edition.* CRC Press (2003).

[16] Sheploak, M. and Dugundji, J., Large deflections of clamped circular plates under initial tension and transitions to membrane behavior, *Journal of Applied Mechanics* (1998) **65**(1): 107.

[17] Faris, W.F., *Nonlinear Dynamics of Annular and Circular Plates under Thermal and Electrical Loadings.* PhD thesis, Virginia Polytechnic Institute and State University, (2003).

[18] Wang, Y.G., Shi, J.L., and Wang, X.Z., Large amplitude vibration of heated corrugated circular plates with shallow sinusoidal corrugations, *Applied Mathematical Modelling* (2009) **33**(9):3523–3532.

[19] Jones, E., Oliphant, T., and Peterson, e., Pearu, SciPy: Open source scientific tools for Python, (2001–).